



Pulsed laser deposition assisted fabrication and characterization of Fe–Co nanoparticles embedded in TiN thin film matrix

D. Kumar^{a,*}, Aarti Sarin^a, Vikram Verma^a, R. Venkatraman^b

^a Department of Mechanical Engineering, North Carolina A & T State University, Greensboro, NC 27411, United States

^b Department of Chemistry, Jackson State University, Jackson, MS 39217, United States

ARTICLE INFO

Article history:

Received 28 October 2011

Received in revised form 10 February 2013

Accepted 11 February 2013

Available online 18 February 2013

Keywords:

Bimetallic nanoparticles

Iron

Cobalt

Single domain magnetic domain

Titanium nitride

Pulsed laser deposition

ABSTRACT

The FeCo material was synthesized in nanoparticle form in a TiN/FeCo/TiN sandwich structure using a pulsed laser deposition (PLD) method. FeCo is significantly cheaper than noble metal based bimetallic materials such as Fe–Pt, Ni–Pd, etc. A Fe_{0.5}Co_{0.5} composition was chosen in this study which is based on the local spin-density electronic-structure calculations. The advantage of this structure is in-situ passivation of FeCo nanoparticles by TiN thin films which is highly stable against atmospheric ambient conditions. TiN/FeCo/TiN samples with variable FeCo nanoparticle size were made by changing the number of laser pulses impinging on a chemically synthesized composite FeCo target. By controlling the particle size in the confined layers, it was possible to tune the magnetic properties from superparamagnetic to ferromagnetic in a controlled way. Magnetic hysteresis characteristics below the blocking temperature are consistent with single-domain behavior.

© 2013 Elsevier B.V. All rights reserved.

1. Introduction

The ever-increasing demand for information storage has pushed research and development of nonvolatile memories, particularly magnetic disk drives and silicon based memories, to areal densities where bit sizes are approaching nanometer dimensions [1–7]. Currently perpendicularly oriented magnetic media disk drive with a typical areal density of 250 Gb/in² is available in the market while the laboratory demonstrations are in the range of 420 to 600 Gb/in². The area corresponding to one bit is typically 80 nm × 20 nm or smaller. Further increase in storage capacity requirements is likely to push bit sizes even smaller, to the point where further scaling of either magnetic thin film or silicon based storage devices becomes very difficult or impossible. A common example is the scaling of magnetic media bits in magnetic hard-disk drives. This scaling is limited by the superparamagnetic phenomenon where the energy required to switch to orientation of a particle's magnetic moment becomes comparable to the particle's thermal energy. The area corresponding to one bit of information is presently approximately 100 nm × 20 nm and contains approximately 50–100 grains with an average diameter of 8 nm. The size of the grains determines the effective signal-to-noise ratio, as the line roughness of the transition between two bits depends on the size of the grains. A reduction of the bit size (and an increase of the areal density) therefore requires a reduction of the average grain size [8]. However, grain volume cannot be reduced arbitrarily; the superparamagnetic

limit is reached at the point when a grain becomes so small that thermal energy alone can flip its magnetization. The critical grain volume, V , that determines the onset of superparamagnetic limit is determined by the condition that the stored magnetic energy, KV , remains about 40–60 times larger than $k_B T$, where K and k_B are the magnetic anisotropy and Boltzmann constants, respectively, and T is the temperature. This implies that size of the thermally stable grains should be larger than approximately 8 nm.

Due to size limitation of nanoparticles in a device that is stable at higher temperatures, efforts are underway to develop and explore materials with larger value of magnetic anisotropy [9–21]. Bimetallic nanomaterials such as Fe–Pt [9,10], Ni–Pt [11,12], Ni–Pd [13], Fe–Ag [14], Au–Co [15], Ag–Ni [16], Ag–Co [16], and Fe–Co [17] have shown promising characteristics in this respect. Fe–Co is significantly cheaper than noble metal based bimetallic materials due to the absence of costly noble metals. Over a wide composition range Fe–Co alloys exist in the bcc-based phase. We have selected Fe_{0.5}Co_{0.5} (FeCo) composition in this study. The selection of these compositions is based on the local spin-density electronic-structure calculations via the layer Korringa–Kohn–Rostoker (LKKR) method [18–20]. The LKKR method, which lies within the atomic sphere approximation and Slater–Pauling curve, suggests that the interatomic exchange coupling and saturation magnetization are nearly at a maximum for the equiatomic FeCo composition. The previous works on bimetallic FeCo magnetic system have focused primarily on nanoparticles in bulk form from [20–22]. In the present study, the FeCo material was synthesized in a nanoparticle form in a thin film based sandwich structure viz. TiN/FeCo/TiN using a pulsed laser deposition method. The thickness of TiN layers separating the FeCo

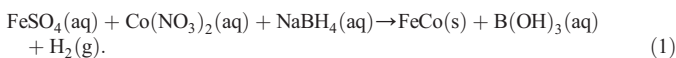
* Corresponding author. Tel.: +336 285 3227.

E-mail address: dkumar@ncat.edu (D. Kumar).

nanoparticle layers has been kept purposely high to prevent interparticle separation. The magnetic interactions are thus only within the interlayer. Another advantage of this structure is in-situ passivation of FeCo by TiN which is highly stable against atmospheric ambient conditions. The laser target to fabricate FeCo nanoparticles was synthesized using a chemical method as opposed to using Fe and Co targets and ablating them alternatively. A chemically synthesized composite FeCo yields nanoparticles with very homogenous elemental distributions.

2. Experimental details

FeCo target was prepared using in-house chemically synthesized FeCo nanoparticle powders. FeCo nanoparticle powders were prepared using a sol gel method where a mixture of aqueous 0.05 M $\text{Co}(\text{NO}_3)_2$ (1.46 g) and 0.05 M FeSO_4 (1.39 g) was reacted with 0.50 M NaBH_4 aqueous solution. The reaction was as follows:



The FeCo nanoparticle, after filtering and drying for elongated period of time at $\sim 100^\circ\text{C}$ was pelletized using stainless steel dye at room temperature. The compacted pellet was sintered at 850°C for 20 h in the $\text{H}_2 + \text{Ar}$ ambient. All the PLD experiments were carried out on (0001) sapphire substrates in high vacuum condition (base pressure $\leq 10^{-7}$ Torr). The other deposition parameters during laser deposition were: laser fluence = $2\text{--}4 \text{ J/cm}^2$, laser pulse repetition rate = 10 Hz, and substrate heater temperature = 600°C . The TiN target used was commercially available. The TiN/FeCo/TiN samples were fabricated in a bilayer structure which could be written as TiN/FeCo/TiN/FeCo/TiN. This configuration was created without breaking vacuum using the multitarget carousel feature of our PLD set-up. Fig. 1 shows the schematic of TiN/FeCo/TiN/FeCo/TiN bilayer structure of the samples used in the present study. The bottom TiN layer, serving as a barrier layer between the substrate and FeCo, was made using 1000 laser pulses on TiN target and the top TiN layer, serving as passive/protective layer, was made using fewer number of laser pulses on TiN target (500 pulse). The two layers of FeCo nanoparticles were separated from each other by TiN layer (also made using 500 pulses of laser on TiN target) which serves as spacer layer between the nanoparticles layers. The thicknesses of TiN layers made using 1000 and 500 pulses correspond to 30 and 15 nm, respectively. These thicknesses were determined using surface profilometer in a separate calibration experiment. TiN/FeCo/TiN/FeCo/TiN samples with variable FeCo nanoparticle size were made by changing the number of pulses impinging on FeCo target and keeping the thickness of TiN layers (barrier layer, spacer layer, and passive layer) fixed. After deposition was complete, the film was left in the chamber until the temperature dropped down to room temperature. Once the temperature reached room temperature, the sample was taken out and characterized for their structural and magnetic properties. The FeCo powder was palletized and sintered at 850°C for 12 h in $\text{Ar} + \text{H}_2$ ambient. Single crystal sapphire (1000) was used as a substrate material. A Bruker AXS D8 discover X-ray diffractometer with a monochromatic CuK_α source of wavelength 0.1545 nm was used to record the X-ray diffraction (XRD) patterns of the samples. Most of the XRD patterns were obtained in thin film mode

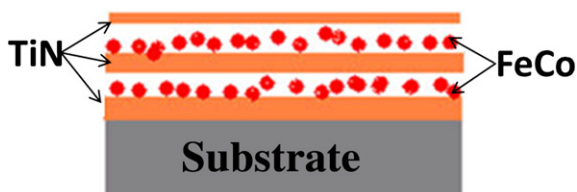


Fig. 1. Schematic FeCo nanoparticle inclusion in TiN thin film matrix in a bilayer configuration represented as TiN/FeCo/TiN/FeCo/TiN. The dimensions of the substrate, TiN film and FeCo nanoparticles are not to the scale.

by sweeping the sample in θ -space, while keeping χ fixed at 90° . Magnetic properties of the samples were measured using a Quantum Design vibrating sample magnetometer (VSM). The zero field cooled (ZFC) magnetization was achieved by applying a small field ranging from 50 to 500 Oe to the sample at 10 K and then warming the sample in the constant field with the magnetization being measured as a function of temperature. The field cooled (FC) magnetization was measured by cooling the sample to 10 K in the presence of 0.4×10^4 to $4 \times 10^4 \text{ A/m}$ field and taking the data while heating the samples up to 300 K. The coercivity of each sample was measured at different temperatures by recording magnetization versus field loops at different temperatures.

3. Results and discussion

FeCo nanoparticles embedded in TiN thin film matrix were structurally characterized using XRD. The results obtained are shown in Fig. 2. The diffraction pattern shows that TiN film as well as FeCo nanoparticles are highly textured with both the materials having the same set of Miller indices, namely (111). Matching the peak positions of (111) planes for TiN and FeCo in the present study with the standard X-ray JSPD data, both the materials were confirmed to have cubic structures. The broad nature of FeCo (111) peak indicates the presence of FeCo system in nanodimensional particle range. Using the Debye–Scherrer's formula, $D = K\lambda/(\Delta(2\theta) \cos \theta)$, the size of FeCo particle (D) was measured to be 9.3, 6.4, and 4.6 nm corresponding to 1000, 750 and 500 pulses. In this formula, $K = 180/\pi$, $\Delta(2\theta)$ is the full width at half maximum (FWHM), and θ is half of the diffraction angle. The particle size could not be estimated for the FeCo 250 pulse sample because the intensity of FeCo was too low to be meaningful. It should be noted that since the values of FWHM of (111) peak of FeCo are significantly higher ($1\text{--}2^\circ$) than the validity range of the Debye–Scherrer's formula, the estimation of particle size using XRD data is quite reasonable. The estimation of particle size by XRD has been confirmed by transmission electron microscopy data of nanoparticle data in our previous studies [23,24]. The peak at 38.2° has been marked with a star sign. This peak arises from the XRD sample stage which is made of Al (JCPDS File No. 00-004-0787). The absence and the presence of this peak depend on the location and physical size of the sample. If the XRD beam is blocked from reaching the samples stage, this peak will be absent.

Fig. 3 shows typical magnetization (M) versus field (H) loops for TiN/FeCo/TiN/FeCo/TiN samples made using 250 laser pulses on FeCo target. M – H loops were also recorded for TiN/FeCo/TiN samples made

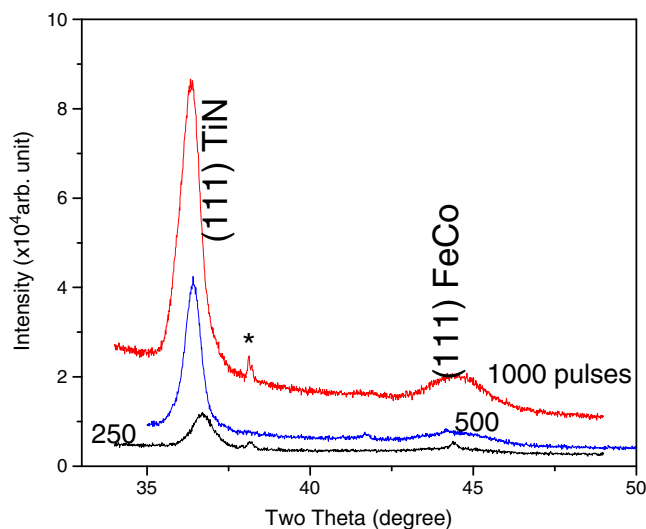


Fig. 2. X-ray diffraction patterns recorded from TiN/FeCo/TiN/FeCo/TiN samples with different nanoparticle sizes. The peak at 38.2° , marked with star sign, comes from the XRD sample stage made of aluminum (JCPDS File No. 00-004-0787).

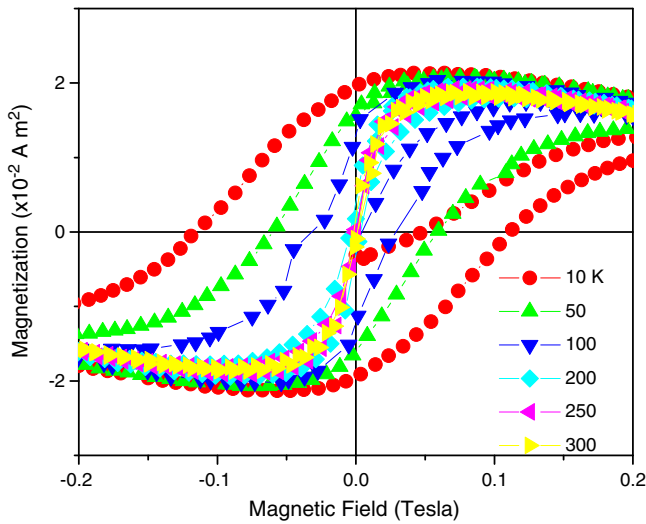


Fig. 3. Magnetization (M) versus field (H) plots for FeCo nanoparticles prepared using 250 laser pulses in a bilayer TiN/FeCo/TiN/FeCo/TiN structure.

using 50, 750, and 1000 laser pulses on FeCo target with fixed thickness (15 nm) of a spacer layer of TiN. All the samples show a similar M–H behavior. According to our previous study on Fe particles embedded in alumina thin film matrix, the possibility of interlayer Fe particle contacts is highly improbable when the spacer layer thickness is beyond 12 nm [24]. Thus, the presence of a 15 nm TiN spacer layer in the present study is logically expected to repudiate the interlayer coupling between the Fe–Co particles in the two layers. The values of coercivity extracted from the MH loops for each sample are plotted in Fig. 4 as a function of number of laser pulses. The solid curves in this figure are just guide to the eyes. As stated earlier, the number of laser pulses directly corresponds to the particle size as found by XRD data and applying Debye–Scherrer’s formula. It is clear from Fig. 4 that there is a distinct maximum in coercivity vs. particle size which is different at different temperatures. These maxima seem to be shifting to higher temperatures. The existence of maxima in coercivity vs. particle size is a well observed phenomenon and has been attributed to transition from single domain to multi domain regions, shown schematically on the two sides of hill. In single domain region, TiN/FeCo (250

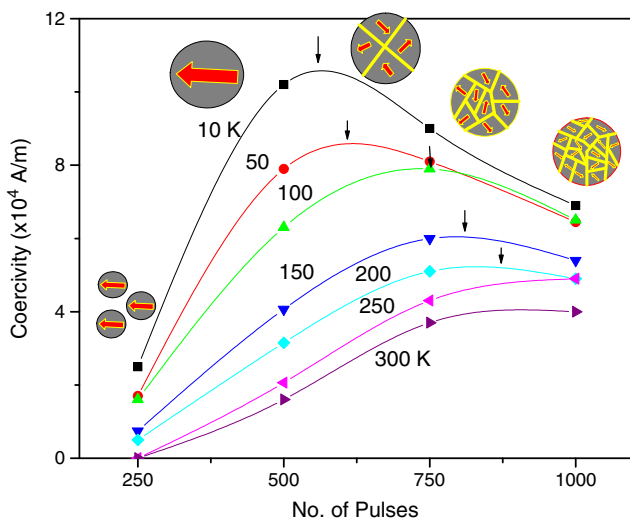


Fig. 4. Coercivity of FeCo nanoparticles prepared using different numbers of laser pulses in a bilayer TiN/FeCo/TiN/FeCo/TiN structure.

pulses)/TiN sample loses hysteretic response around 250 K and above this temperature. The loss in hysteresis suggests that energy barrier ($= 25k_B T$) for spin flip for this sample is $48 \times 10^3 \text{ J/m}^3$ at 250 K corresponding to particle size of 3.5 nm, which was estimated by extrapolating the measured particle size and number of laser pulses.

The coercivity values at different temperatures, extracted from the M–H loops of the TiN/FeCo/TiN, are plotted in Fig. 5. It is apparent from this figure that the coercivity is strongly dependent on temperature. This is because in order for a particle to reverse its spin, it should have enough thermal energy to surmount the energy barrier $\Delta E = KV$ for the reversal. The energy barrier for the reversal is the difference the maximum and minimum values of the total energy (E). At higher temperature, the particles have higher thermal energy, and hence, they require smaller field to reverse the magnetization. This field is equal to H_c and is given by

$$H_c = 2 k/M_s \left[1 - (25k_B T/KV)^{1/2} \right]. \tag{2}$$

When T approaches zero, H_c approaches $2 K/M_s$ i.e., $H_{c,0} = 2 K/M_s$. For particles of constant size there is a temperature, called the blocking temperature, T_B , at which the metastable hysteretic response is lost for a particular experimental time. For uniaxial particles T_B can be taken as $KV/25k_B$. Substituting the value of T_B and $H_{c,0}$ in Eq. (1), we get

$$H_c = H_{c,0} \left[(1 - T/T_B)^{1/2} \right]. \tag{3}$$

As shown in the inset of Fig. 6, the FeCo particles, for example, in sample TiN/FeCo (500 pulses)/TiN/FeCo (500 pulses)/TiN follow closely this relationship. It is clear from this figure that the fitting is pretty satisfactory and the values of parameters such as $H_{c,0}$ and T_B are very reasonable. For example, the value of $H_{c,0}$ and T_B from this fit are found to be 1225 and 400 K, respectively for FeCo (500 pulses) sample. Substituting the values of T_B (400 K), magnetic anisotropy K ($48 \times 10^3 \text{ J/m}^3$) for FeCo, and the Boltzmann constant k_B ($1.38 \times 10^{-23} \text{ J/K}$) in the expression for $T_B = KV/25k_B$, we find the mean radius of FeCo particles to be 3.6 nm in TiN/FeCo (500 pulses)/TiN sample. This is in good agreement with the particle size measured using XRD studies (4.6 nm). In all the samples, the values of particle size measured and calculated also agree with each other reasonably well. The superior properties of FeCo system over individual metals is attributed to substitution of 50% of Fe atoms by Co atoms in the unit cell, say, bcc. This substitution leads to modification in crystal

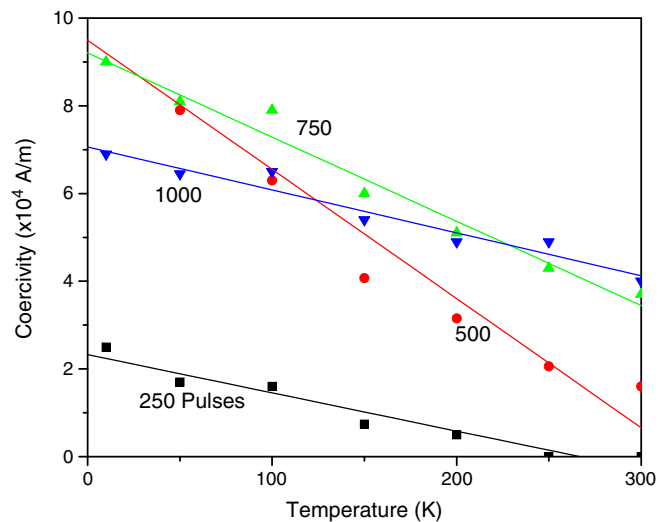


Fig. 5. Plots of coercivity as a function of temperature for TiN/FeCo/TiN/FeCo/TiN bilayer samples with variable FeCo particle sizes made using 250, 500, 750, and 1000 pulses on FeCo target.

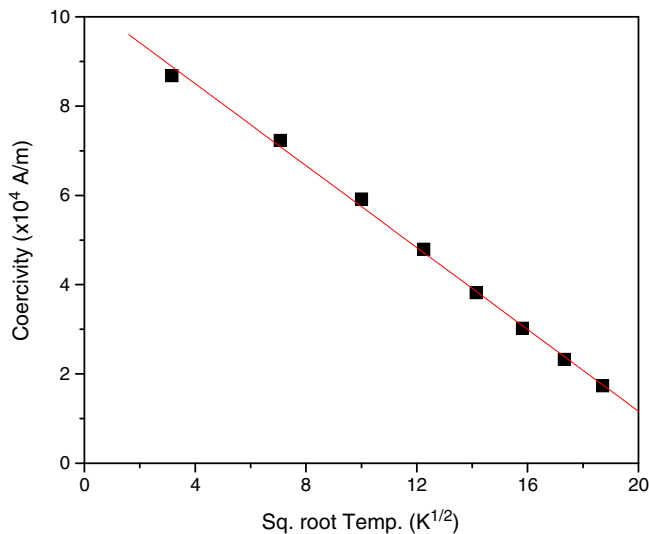


Fig. 6. A linear fit of coercivity versus square root of temperature data for TiN/FeCo (500 pulses)/TiN/FeCo (500 pulses)/TiN samples.

field splitting of d -orbital, and hence, there is change in the occupancy of both majority and minority states. Assuming both Fe ($3d^6$) and Co ($3d^7$) to be in high spin state (i.e. pairing energy is more than crystal field splitting), the hybridization of $d(\text{Fe})$ and $d(\text{Co})$ atomic orbitals leads to formation of bonding and antibonding molecular orbitals. Due to repulsion between Fe d and Co d electrons, the separation between the bonding (e_g) and antibonding (t_{2g}^*) molecular orbitals is larger than the crystal field splitting in pure metals which is shown schematically in Fig. 7. Due to larger separation e_g and t_{2g}^* , the electrons in e_g first get paired and then the rest of electrons fill the t_{2g}^* orbitals singly. In this situation the number of unpaired electrons (n) per Co molecule is 5 versus $n = 4$ and $n = 3$ per atom in Fe and Co, respectively. The change in Fe properties upon substitution by 50% Co can be explained by transformation from a weak ferromagnet (i.e. both majority- and minority-spin d states, $d \uparrow$ and $d \downarrow$, are only partially occupied for pure Fe) to a strong ferromagnet ($d \uparrow$ state becomes fully occupied (Fig. 7)). This transformation is progressive because $d(\text{Fe})$ – $d(\text{Co})$ hybridization is weaker than $d(\text{Fe})$ – $d(\text{Fe})$ hybridization, as the Co d -shell is more localized than the Fe d -shell due to one more

proton in the Co nucleus and outer electron still being in the same energy shell ($3d$).

4. Conclusions

Presently a wide spread of research activities is pursued in the area of nanostructured materials in order to synthesize materials with improved properties so that the performance of nanostructured components in actual devices could be improved. The key to the effective fabrication of these nanostructured materials with improved properties is the development of smart materials by material-engineering and understanding the fundamentals of materials science. In this context we have developed a smart thin film processing method based upon pulsed laser deposition to process nanocrystalline materials with accurate size and interface control with improved magnetic properties. Using this method, single domain nanocrystalline FeCo particles in 2–10 nm size range embedded in crystalline TiN have been produced. By controlling the particle size in the confined layers, it was possible to tune the magnetic properties from superparamagnetic to ferromagnetic in a controlled way. Magnetic hysteresis characteristics below the blocking temperature are consistent with single-domain behavior. The present results are important from fundamental as well as a technological point of view. The fundamental understandings are related to existence of single and multidomain domain regions as a function of temperature. The improvement in magnetic properties has been explained on the basis of availability of larger number of unpaired electrons in accordance with crystal field assisted filling of majority and minority spin states. The precision in nanoparticle size control and their inclusion in a crystalline and highly conductive medium could promote integration of magnetic and electronic devices into one compact system. This research has circumvented the scaling challenges of conventional technologies by effectively exploiting the benefits of nanomaterials in conjunction with a different method and a material (FeCo) which is relatively cheaper than other bimetallic materials based on noble metal such as Ni–Pt, Fe–Pt, Ni–Pd, Fe–Ag, Au–Co, and Ag–Ni.

Acknowledgment

This work was supported by the National Science Foundation-NIRT (DMR-0403480), NUE (EEC 0939344) and by the NSF Engineering Research Center grant at North Carolina A & T State University.

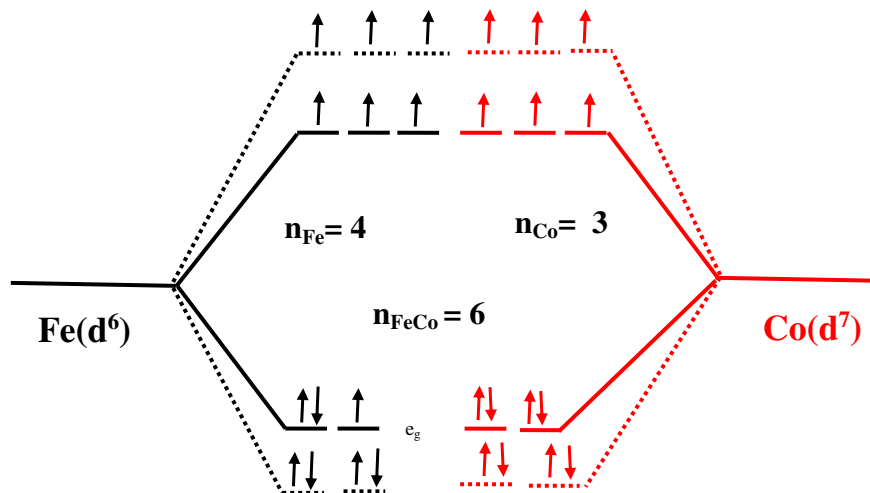


Fig. 7. Schematic of formation of bonding and antibonding (*) molecular orbitals in FeCo molecule, n is the number of unpaired electrons in pure Fe and Co metals and FeCo alloy. Solid line is for atomic orbital (black = iron, red = cobalt) and dotted line is for molecular orbital.

References

- [1] C. Stamm, F.A. Marty, V.S. Weich, E.U. Maier, U. Ramsperger, H. Fuhrmann, D. Pescia, *Science* 282 (1998) 449.
- [2] E. Gu, E. Ahmad, S.J. Gray, C. Daboo, J.A.C. Bland, L.M. Brown, J.C. Chapman, *Phys. Rev. Lett.* 78 (1997) 1158.
- [3] D. Kumar, H. Zhou, T.K. Nath, A.V. Kvit, J. Narayan, *Appl. Phys. Lett.* 79 (2001) 2817.
- [4] G.A. Prinz, *Science* 282 (1998) 1660.
- [5] C.B. Murray, C.R. Kagan, M.G. Bawendi, *Science* 270 (1995) 1335.
- [6] A.P. Alivisatos, *Science* 271 (1996) 271.
- [7] R.P. Andres, T. Bein, M. Dorogi, S. Feng, J.I. Henderson, C.P. Kubiak, W. Mahoney, R.G. Osifchin, R. Reifenger, *Science* 272 (1996) 1323.
- [8] S.A.M. Tofail, I.Z. Rahman, M.A. Rahman, *Appl. Organomet. Chem.* 15 (2001) 373.
- [9] V.T. Volkov, V.I. Levashov, V.N. Matveev, V.A. Berezin, *Appl. Phys. Lett.* 91 (2007) 26511.
- [10] B. Bian, D. Laughlin, K. Sato, Y. Hirotsu, *J. Appl. Phys.* 87 (2001) 6962.
- [11] R. Krishnan, H. Lassri, S. Prasad, M. Portes, M.J. Tesser, *J. Appl. Phys.* 73 (1993) 6433.
- [12] C.E. Dahmani, M.C. Cadville, J.M. Sanchez, J.L. Moran-Lopez, *Phys. Rev. Lett.* 55 (1985) 1208.
- [13] N. Nunomura, H. Hori, T. Teranishi, M. Miyake, S. Yamada, *Phys. Lett. A* 249 (1998) 524.
- [14] Y. Kobayashi, K. Honda, Y. Akoi, H. Sata, T. Ono, T. Shinjo, S.A. Makhlof, K. Sumiyama, K.J. Suzuki, *Mag. Mag. Mater.* 176 (1997) 164.
- [15] M.J. Kitada, *Mag. Mag. Mater.* 208 (2000) 244.
- [16] D.J. Kubinski, J.J. Holloway, *J. Appl. Phys.* 77 (1995) 782.
- [17] H.F. Li, R.V. Ramanujan, *Trans. Indian Inst. Met.* 56 (2005) 965.
- [18] J.M. MacLaren, S. Crampin, D. Vedensky, *Phys. Rev. B* 40 (12) (1989) 176.
- [19] P.R. James, M. MacLaren, D.K. Saldin, *Phys. Rev. B* 57 (1998) 2621.
- [20] A. Diaz-Ortiz, R. Drautz, M. Fahnle, H. Dosch, J.M. Sanchez, *Phys. Rev. B* 73 (2006) 224208.
- [21] J.M. MacLaren, T.C. Schulthness, W.H. Buttler, R. Sutton, M. McHenry, *J. Appl. Phys.* 85 (1999) 4833.
- [22] R.F. Sabiryanov, S.K. Bose, O.N. Mryasov, *Phys. Rev. B* 51 (1995) 8958.
- [23] H. Zhou, D. Kumar, A. Kvit, A. Tiwari, J. Narayan, *J. Appl. Phys.* 94 (2003) 4841.
- [24] N. Hendon, J. Abiade, S. Oh, S.J. Pennycook, D. Kumar, *J. Appl. Phys.* 103 (2008), (10307D515).